JOURNAL OF MATERIALS SCIENCE 24 (1989) 562–568

Application of transmission electron microscopy and X-ray diffraction to the study of the crystallography of unidirectionally solidified NiO–ZrO_2(CaO) eutectic

H. LAROUI, M. DECHAMPS, G. DHALENNE, A. REVCOLEVSCHI
Laboratoire de Chimie des Solides, UA CNRS 446, Université Paris Sud, Bât. 414, 91405 Orsay Cedex, France

A lamellar NiO–ZrO_2(CaO) eutectic has been studied by X-ray diffraction techniques and transmission electron microscopy in order to characterize its crystallography (orientation relation between phases and indexations of interlamellar plane and growth direction) and to compare the information which results from both methods. X-ray techniques have indicated an orientation relation (1 0 0) [0 0 1] ZrO_2 ∥ (1 1 1) [1 $\bar{1}$ 0] NiO associated with a lamellar interface (1 0 0) ZrO_2 ∥ (1 1 1) NiO and with a growth direction [0 0 1] ZrO_2 ∥ [1 $\bar{1}$ 0] NiO. Transmission electron microscopy has confirmed this orientation relation (adopted by about 80% of the lamellae) as well as the orientation of the lamellar plane. Growth directions, however, were not as systematically well-defined as expected from the X-ray study. In addition, a minor homogeneous population (10% of the lamellae) corresponding to (*h k l*) [*u v w*] ZrO_2 ∥ (*h k l*) [*u v w*] NiO was also observed.

1. Introduction

Microstructures of unidirectionally solidified eutectics generally consist of either rods of one of the two phases distributed uniformly in a matrix of the second, or of alternating plates of the two eutectic phases, depending on their relative volume fraction. In both cases, the discontinuous rods or plates are distributed in a regularly spaced array with their longer dimension oriented in the direction of the solidification and normal to the solid–liquid interface. It has been established that in most unidirectionally solidified eutectics, specific crystallographic relations exist between the two phases [1–3].

The purpose of this study was to characterize crystallographically the lamellar oxide–oxide eutectic NiO–ZrO_2(CaO) by both transmission electron microscopy and X-ray diffraction techniques in order to compare the information obtained by the two methods.

After a brief account of the experimental technique used to grow the material, and after a discussion of the main features of the microstructure which was obtained, the crystallographic characteristics of the eutectic samples are examined.

2. Growth technique and eutectic microstructure

2.1. Growth

In the absence of any available nickel oxide–zirconia phase diagram, a metallographic study was carried out in order to determine the exact eutectic composition. Several mixtures of NiO, ZrO_2 and CaO high-purity powders (> 99.99%) were considered. The proportion of CaO relative to ZrO_2 was fixed uniformly at 15 mol % to obtain a stabilized cubic zirconia. Micrographic observation of the structures corresponding to the different samples indicated regular eutectic microstructures, free from primary phases, for a composition of 70 mol % NiO–25.5 mol % ZrO_2 and 4.5 mol % CaO. This composition corresponds to a volume fraction of about 45% for the ZrO_2 phase.

Unidirectional solidification was carried out by a floating zone method associated with a biellipsoid image furnace described in detail elsewhere [4, 5]. Growth experiments were performed in air, at a solidification rate of 15 mm h^{-1}, using cylindrical bars sintered in air at 1200° C for 24 h. The temperature gradient was about 600° C cm^{-1} at the solid–liquid interface. The resulting samples were several cm long and ≈ 1 cm diameter. Their structure is lamellar, in good agreement with the theory of Hunt and Chilton [6] which predicts that lamellar, rather than rod-type structures, are stable when the volume fraction of the minor phase is higher than 32%.

2.2. Microstructures

In the floating zone method, the curvature of the solidification front which is convex towards the liquid, defines the orientation of the lamellae, which are well aligned with the heat-flow direction. This results in a structure which consists of a core made of lamellae aligned parallel to the rod axis, and peripheral regions where lamellae are inclined up to 20° with respect to the rod axis. The lamellae grow parallel to each other

0022–2461/89 $03.00 + .12

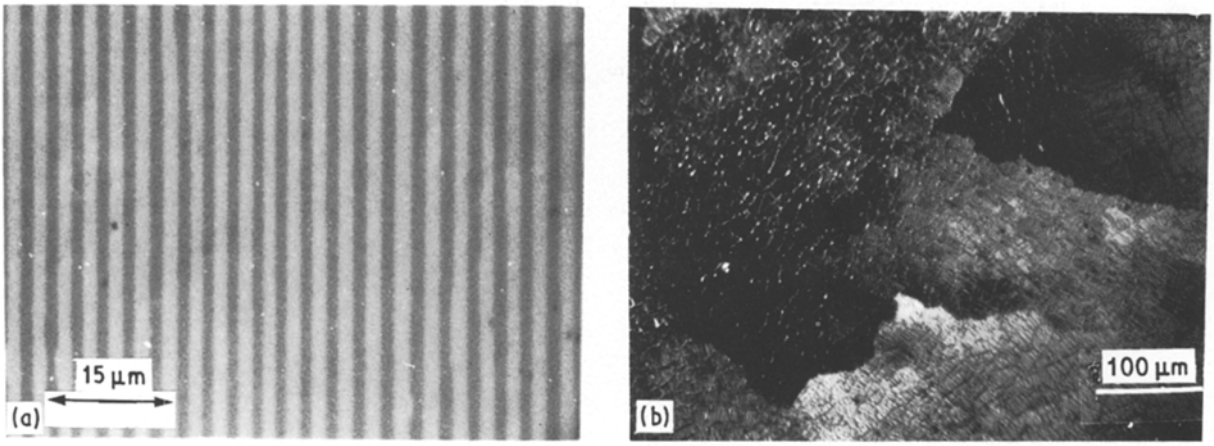

Figure 1 Optical micrographs of directionally grown NiO–ZrO_2(CaO) eutectic: (a) longitudinal section, (b) transverse section. (The wavelets result from ion-milling.)

in small domains often considered as "grains" (Fig. 1a). The core domains of 30 to 300 μm diameter, are very elongated along the direction of the ingot axis (length/diameter $\approx$ 10) and are slightly rotated with respect to each other.

Transverse sections show microstructures made of such domains (Fig. 1b), each of them containing 15 to 150 pairs of parallel lamellae. The domains are separated by surfaces made of fault lines. Two types of defects are generally associated with the presence of these fault lines. On the one hand, a net fault, when a region one side of the line contains one extra lamella with respect to the other, on the other hand, a no-net fault, when the number of lamellae on each side of the fault line is equal. Both types of fault are usually normal to the solid–liquid interface. Within grains, one can also observe lamellar terminations, i.e. extra lamellae which are the origin of perturbations across several lamellae. Similar faults have been reported in several other binary metallic and ceramic eutectic systems [1, 7, 8].

The interlamellar spacing, λ, was measured on sections normal to the specimen axis and the relationship $\lambda = AR^{-2}$ [9] where A is a constant and R the solidification rate, was verified (Fig. 2).

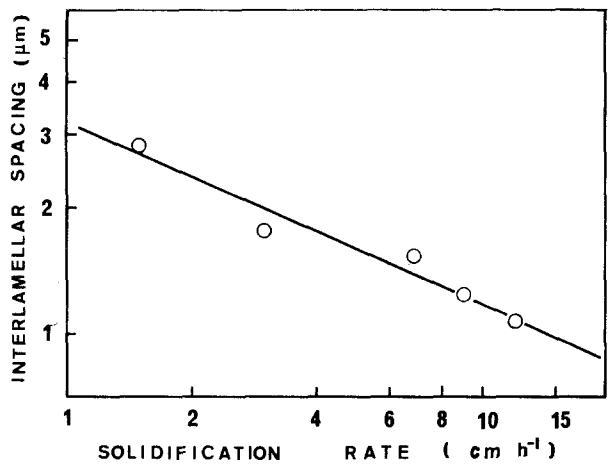

Figure 2 Interlamellar spacing (λ) plotted against solidification rate (R).

3. X-ray diffraction studies

Laue back-reflexion X-ray photographs, taken on transverse sections with the rod axis parallel to the X-ray beam, show elongated spots indicating a well-defined texture. The asterism of the spots reveals that scatter can reach 20°, which is consistent with the microstructural observations.

Comparison of X-ray diffractograms of eutectic transverse sections and of powder diagrams of the same specimen indicates strongly oriented samples (Fig. 3).

These techniques, however, are too macroscopic to give precise local information, because of the mis-

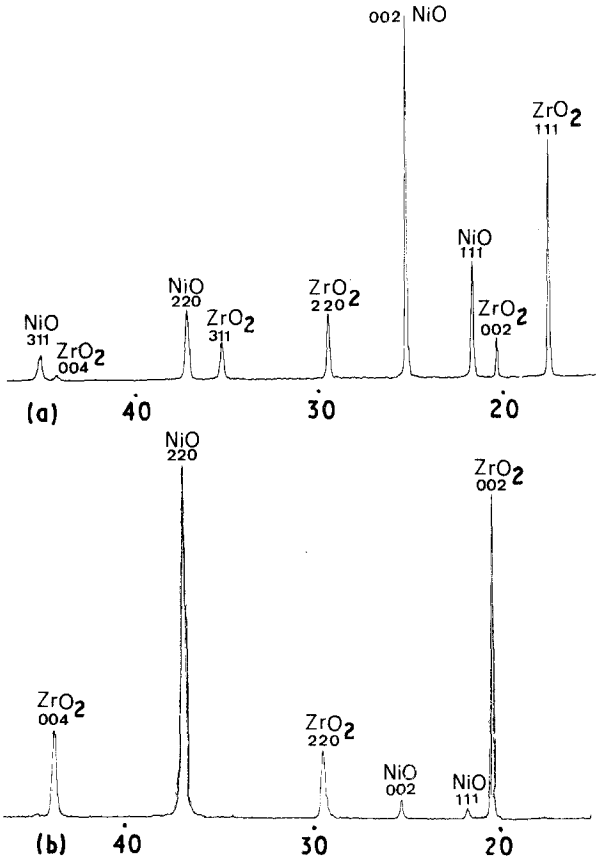

Figure 3 Comparison of X-ray diffraction patterns of (a) powder and (b) eutectic transverse section. X-ray line relative intensities indicate a preferential growth direction in both phases: ⟨0 0 1⟩ for ZrO_2 and ⟨1 1 0⟩ for NiO.

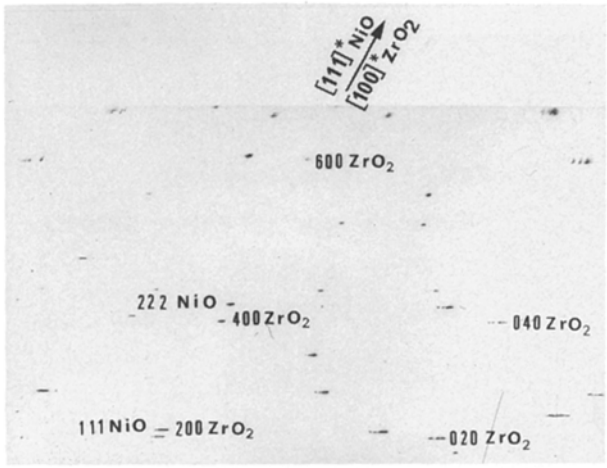

Figure 4 Weissenberg zero-level photograph normal to the growth direction ($[0\,0\,1]ZrO_2 \parallel [1\,\bar{1}\,0]NiO$). The parallelism between $[1\,0\,0]^* ZrO_2$ and $[1\,1\,1]^*$ NiO rows is observed [10].

orientation existing between domains. To overcome this limitation, microfragments including about one hundred pairs of lamellae of the two phases were studied by rotating crystal, Weissenberg and Buerger precession methods (Figs 4 and 5). Such microfragments were thought to contain a very small number of domains, possibly only one domain in the most favourable cases. They were selected from the core of the ingots where the rod axis and the plane of the lamellae are expected to be parallel. This axis was systematically aligned with the rotation axis of the cameras.

Crystallographic data obtained from several lamellar specimens grown at $1.5\,cm\,h^{-1}$ have revealed reproducible characteristics; the lamellae can be considered as consisting of two interpenetrating single crystal systems, whose orientation relationship is described by

$$\begin{aligned}(1\,1\,1)\ NiO &\parallel (1\,0\,0)\ ZrO_2(CaO)\\ [1\,\bar{1}\,0]\ NiO &\parallel [0\,0\,1]\ ZrO_2(CaO)\end{aligned} \qquad (A)$$

A careful examination, by optical microscopy, of the orientation of the lamellae with respect to the polished faces of the microfragments added to the information obtained from the corresponding Weissenberg photographs, has allowed us to show that the interface planes are, within experimental error, very close to $(1\,1\,1)\,NiO \parallel (1\,0\,0)\,ZrO_2$. Buerger precession patterns obtained when the X-ray beam is perpendicular to these interfaces indicate that the growth direction, included in the interface plane, is $[1\,\bar{1}\,0]$ for NiO and $[0\,0\,1]$ for ZrO_2 [10]. The above-mentioned orientation relation is the same as that already observed in lamellar eutectics such as NiO–Y_2O_3 [11] and MgO–ZrO_2 [12] which also associate cubic phases of fcc and fluorite structure types.

Occasionally, a second orientation relation was found

$$\begin{aligned}(1\,1\,1)\ NiO &\parallel (1\,0\,0)\ ZrO_2(CaO)\\ [2\,\bar{3}\,1]\ NiO &\parallel [0\,1\,3]\ ZrO_2(CaO)\end{aligned}$$

In this case, growth directions of NiO and ZrO_2 are $[2\,\bar{3}\,1]$ and $[0\,1\,3]$, respectively, and the interface is $(1\,1\,1)\,NiO$ parallel to $(1\,0\,0)\,ZrO_2$.

In fact, the two misorientation relations which we have found are identical, within 0.7°. The only difference observed concerns growth directions. The existence of several growth directions for one unique relative orientation of eutectic phases and one unique type of interface has already been reported in other oxide–oxide systems [13, 14].

Nevertheless, Weissenberg (Fig. 4) and Buerger photographs (Fig. 5) indicate a scatter of the diffraction spots which shows, within the microfragments under study, the existence of domains misoriented by a few degrees (≈ 10). Thus, the main drawback of these X-ray diffraction methods is that the area of illumination and the fragment under study are sufficiently large to include several misoriented domains.

4. Transmission electron microscope study

4.1. Method

In order to assess more accurately the data of the X-ray study, transmission electron microscopy was performed to obtain local crystallographic information from couples of adjacent lamellae within well-defined eutectic domains. The orientation relation existing between the two phases was determined on several thin foils prepared from nine different ingots. Thin electron transparent specimens were prepared by sectioning the ingots into discs, 1 mm thick, which

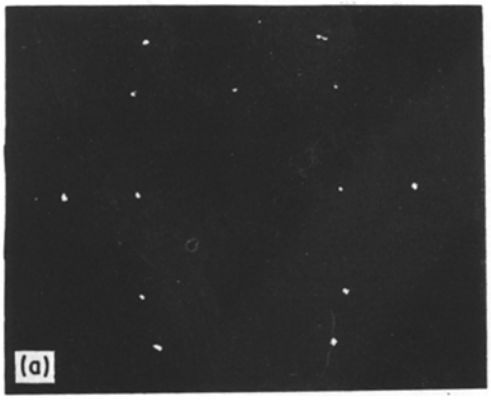

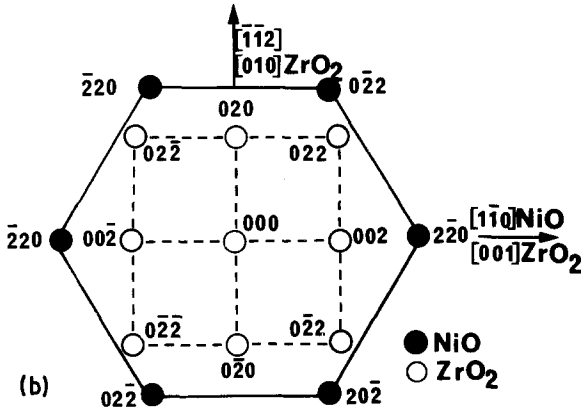

Figure 5 Buerger pattern and corresponding reciprocal plane indexation for NiO–ZrO_2(CaO) eutectic. The plane represented is normal to $[1\,1\,1]$ for NiO and $[1\,0\,0]$ for ZrO_2. The sample is oriented along the growth direction: $[1\,\bar{1}\,0]$ for NiO and $[0\,0\,1]$ for ZrO_2.

were thinned by mechanical grinding before ion-milling. The estimated final thickness of the observed areas was about 100 nm. The two phases exhibited different thinning rates, with NiO thinning much faster than ZrO_2. The specimens chosen for observation were prepared from the core of the ingots where, as already stated, lamellar interfaces, and growth directions are closely parallel to the axis of the ingots. This procedure yields the growth direction by determining the crystallographic direction normal to the plane of the thin foil. Seventy interlamellar boundaries were characterized by TEM. In each case, the orientation relation, the lamellar interface plane, and the growth direction were determined.

The geometrical relation existing between any two adjacent crystals is described by considering the matrix product (M) of a rotation (M_{rot}), which describes the orientation relationship *stricto sensu*, and of a deformation (M_{def}), which takes into account the crystallographic parameters of both crystals

$$M = M_{rot} \cdot M_{def} \quad (1)$$

In the case of the lamellar structure under study, both crystals are cubic (f c c) and the deformation is reduced to a simple expansion which can be computed from the lattice parameters of both phases ($a_{NiO} = 0.418$ nm and $a_{ZrO} = 0.512$ nm). Thus the deformation can be written as a diagonal matrix:

$$M_{def} = \begin{vmatrix} \varepsilon & 0 & 0 \\ 0 & \varepsilon & 0 \\ 0 & 0 & \varepsilon \end{vmatrix}$$

ε is the deformation coefficient and $M = \varepsilon \cdot M_{rot}$, with $\varepsilon = 0.28$ if the transformation is carried out from the NiO lattice to the ZrO_2 lattice.

The interlamellar orientation relationship M_{rot} can be expressed by 24 equivalent descriptions which were computed, for each pair of lamellae, by using a matrix method originally proposed by Lange [15] and recently applied to TEM by several authors [16–20]. Basically, the method consists of characterizing each lamellar crystal by three non-coplanar crystallographic directions which define the transformation matrix M from the $\langle 0\,0\,1 \rangle$ orthonormal trihedron of the crystal to the experimental crystalline trihedron. Simultaneously, the three corresponding pairs of angles read on the goniometer stage of the microscope give access to the spherical coordinates of each experimental direction in a fixed orthonormal trihedron. Thus, the transformation matrix M' from the reference trihedron to the experimental trihedron, is defined. Hence, the matrix product given below defines the transformation matrix from the reference trihedron to the $\langle 0\,0\,1 \rangle$ trihedron of lamella 1.

$$M_1 = M' \cdot M^{-1}$$

If M_2 is the equivalent matrix corresponding to lamella 2, we can then define the experimental matrix which expresses the rotation between the two adjacent lattices, as

$$M_{rot} = (M_2)^t \cdot M_1 \quad (2)$$

The rotation angle is calculated from the trace of M_{rot} and the rotation axis is an eigen vector of M_{rot}. The 24 equivalent descriptions associated with the cubic symmetry are obtained by permuting the elements of M_2. The uncertainty of this determination was shown to be less than 3% of the misorientation angle [21].

The crystallographic orientation of the interlamellar plane is determined by indexing the trace of the interlamellar boundary when the thin foil is horizontal. The method is based upon the assumption that the boundaries are parallel to the electron beam when the foil is horizontal in the microscope. The uncertainty of the determination is less than 10°. The growth direction is obtained by indexing the normal to the plane of the thin foil. The uncertainty of the determination is less than 15°, including the uncertainty due to the metallographic preparation of the sample.

As will be seen in the next section, the results of the X-ray study are statistically verified. However, there is an important scatter of the orientation relationships. To obtain a quantitative insight of this dispersion, the deviation angle between each rotation matrix, M_{rot}, deduced by electron diffraction and the rotation matrix corresponding to Relation A, i.e.

$$M_{X\text{-ray}} = \begin{vmatrix} 3^{1/2}/3 & -3^{1/2}/3 & 3^{1/2}/3 \\ 2^{1/2}/\sqrt{3^{1/2}} & 6^{1/2}/6 & -6^{1/2}/6 \\ 0 & 2^{1/2}/2 & 2^{1/2}/2 \end{vmatrix} \quad (3)$$

was computed according to the standard procedure of the matrix calculation. The matrix (M_{dev}) which expresses the deviation is

$$M_{dev} = M \cdot (M_{X\text{-ray}})^{-1} \quad (4)$$

where $(M_{X\text{-ray}})^{-1}$ is the inverse of $M_{X\text{-ray}}$. The deviation angle, θ, is deduced from the trace of M_{dev} using

$$\theta = a\cos\left[\frac{1}{2}\left(\sum_1^3 s_{jj} - 1\right)\right] \quad (5)$$

4.2. Results

4.2.1. Orientation relation

The determination of the orientation relationships existing between two adjacent lamellae has been made

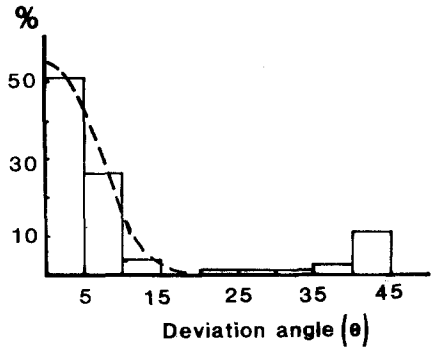

Figure 6 Fraction of orientation relationships plotted against deviation angle, assuming that there is only one homogeneous population corresponding to Relation 3. The large maximum shows the existence of a well-defined preferential orientation relation, A. The second maximum includes the orientation relations which do not fit A (populations B and C).

TABLE I Distribution of orientation relations. (N = population, σ = standard deviation.) It is recalled that 68% and 95% of the elements of a normal distribution will lie within $\pm\sigma$ and $\pm 2\sigma$, respectively, of the mean value of the population

Total		Population A $M_{rot} = \begin{vmatrix} 3^{1/2}/3 & -3^{1/2}/3 & 3^{1/2}/3 \\ 2^{1/2}/3^{1/2} & 6^{1/2}/6 & -6^{1/2}/6 \\ 0 & 2^{1/2}/2 & 2^{1/2}/2 \end{vmatrix}$			Population B $M_{rot} = \begin{vmatrix} 1 & 0 & 0 \\ 0 & 1 & 0 \\ 0 & 0 & 1 \end{vmatrix}$			Population C M_{rot} = undefined	
N	σ (deg)	N	%	σ (deg)	N	%	σ (deg)	N	%
70	18.2	57	81.4	5.5	8	11.4	6.5	5	7.1

on interlamellar boundaries belonging to different domains, because it was shown that all the lamellae in one domain exhibit the same orientation relation, within a few degrees. The conclusions of the study carried out to characterize the deviation from a specific orientation relation, by using Equations 4 and 5 are collected together in Table I.

The gaussian curve centred on the ordinate axis of Fig. 6 confirms unambiguously the existence of a strong trend for the lamellae to adopt the orientation Relation A defined by the matrix $M_{X\text{-ray}}$ (Relation 3). About 80% of the orientation relationships are within 10° from this relation, deduced from the X-ray study; the remaining 20% differ by a much larger amount. The shape of the histogram clearly indicates the existence of other orientation relations. A closer analysis of the high deviation matrix population yields evidence of a second preferential orientation relation, which is characterized by a unit rotation matrix M_{rot}, corresponding to

$$\begin{aligned} &(h\,k\,l)\ \mathrm{NiO} \parallel (h\,k\,l)\ \mathrm{ZrO_2(CaO)} \\ &[u\,v\,w]\ \mathrm{NiO} \parallel [u\,v\,w]\ \mathrm{ZrO_2(CaO)} \end{aligned} \qquad \text{(B)}$$

Figs 7a, b, c and d show typical lamellar crystals belonging to the populations characterized by Relations A and B, respectively, and the corresponding diffraction patterns. Five orientation relations are unclassifiable (population C).

The homogeneity of populations A and B was verified by determining the standard deviation (σ) of each one, and comparing these with the standard deviation of the whole population by assuming that there was only one preferential orientation relation defined by the matrix $M_{X\text{-ray}}$ (Relation 3). 68% of the lamellae corresponding to the major orientation Relation A and to Relation B are within σ = 5.5° and 6.5° of their respective "ideal" orientation relation.

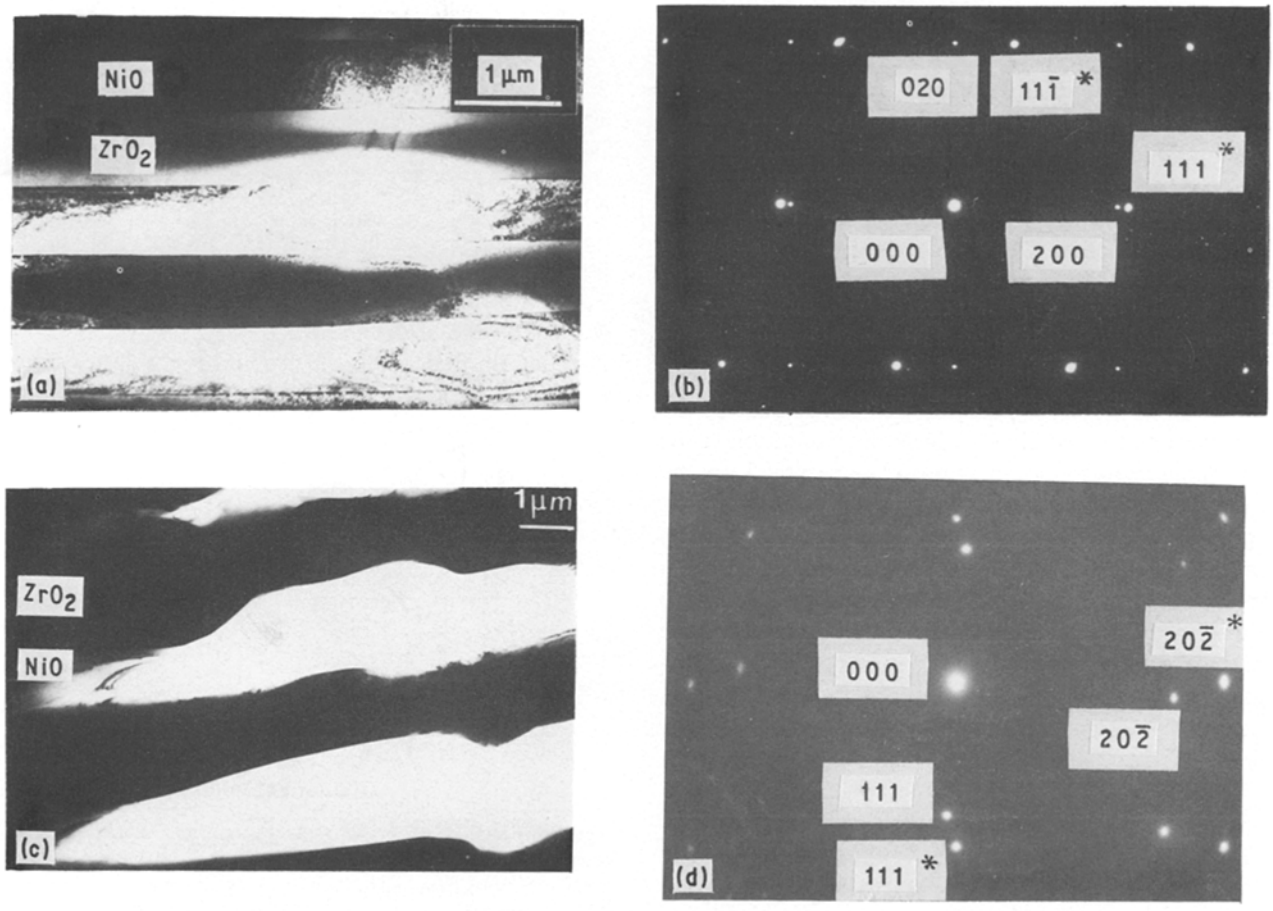

Figure 7 Comparison of populations A (left) and B (right). (a), (c) Transmission electron micrographs of lamellae; (b), (d) corresponding microdiffraction patterns with superimposed zone axis typical of relations A and B.

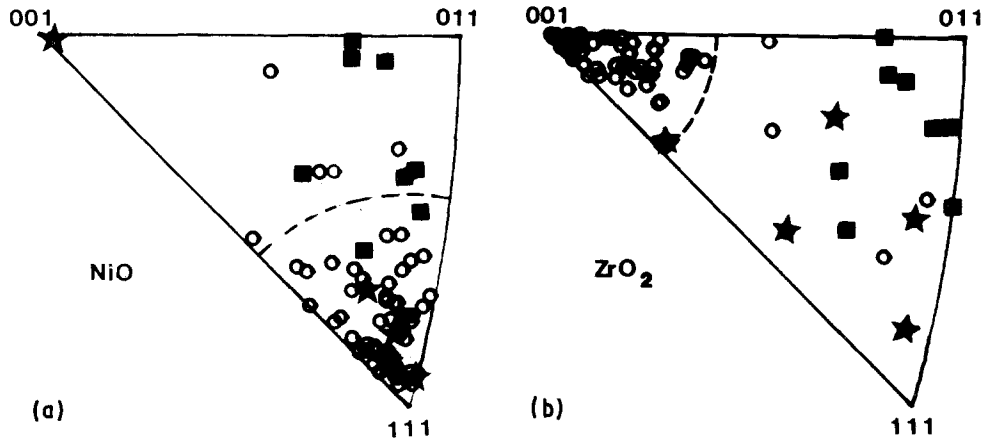

Figure 8 Distribution of the interlamellar planes indexed relative to NiO and ZrO_2. Interfaces corresponding to (○) Relation A, (■) Relation B, and (★) undefined C.

TABLE II Distribution of interlamellar planes and growth directions for populations A, B and C. (N = population; σ = standard deviation.) Only the poles located within the dashed curve of Fig. 8 were taken into account to calculate σ for population A

Population distribution with respect to	Interlamellar plane						Growth direction					
	A			B		C	A			B		C
	N	%	σ (deg)	N	%	N	N	%	σ (deg)	N	%	N
NiO	52	74.2	9.7	8	11.4	10	57	81.4	18.6	8	11.4	5
ZrO_2	53	75.7	9.6	8	11.4	10	57	81.4	24.9	8	11.4	5

Conversely, σ would be equal to 18.2°, if all the lamellae were considered as belonging to population A.

4.2.2. Interlamellar plane

The poles of the boundaries, indexed relative to both NiO and ZrO_2 adjacent phases, are reported on two stereographic triangles (Fig. 8). With few exceptions the boundaries of population A appear to be very homogeneous in orientation, with crystallographic indices close to those found by X-ray diffraction, namely (1 1 1) for NiO (σ = 9.7°) and (0 0 1) for ZrO_2 (σ = 9.6°), (see Table II).

Population B is not, in terms of nature of interface plane, as homogeneous as population A. Indeed, the preferential interlamellar plane observed for population A is incompatible with Relation B and the general trend which appears for population B, (0 1 1) NiO ‖ (0 1 1) ZrO_2 is far from being well-defined (σ_{NiO} = 15.5°; σ_{ZrO} = 13.8°).

4.2.3. Growth direction

The directions normal to the thin foil are expected to be representative of the growth direction of each phase. In each domain this direction was indexed with respect to NiO and ZrO_2. The resulting data are reported in standard stereographic triangles (Fig. 9). For each population considered, one can note a very large scatter of the growth direction (Table II). In fact, any direction contained in the interface plane can be parallel to the growth direction. However, the distribution is not fully homogeneous and a larger density of growth directions is observed in population A near ⟨1 2 3⟩ for NiO and ⟨3 1 0⟩ for ZrO_2, and in population B in the vicinity of ⟨1 1 1⟩.

5. Conclusions

X-ray diffraction techniques applied to the study of the lamellar eutectic NiO–ZrO_2(CaO) have permitted us to establish a unique orientation relation, A, between

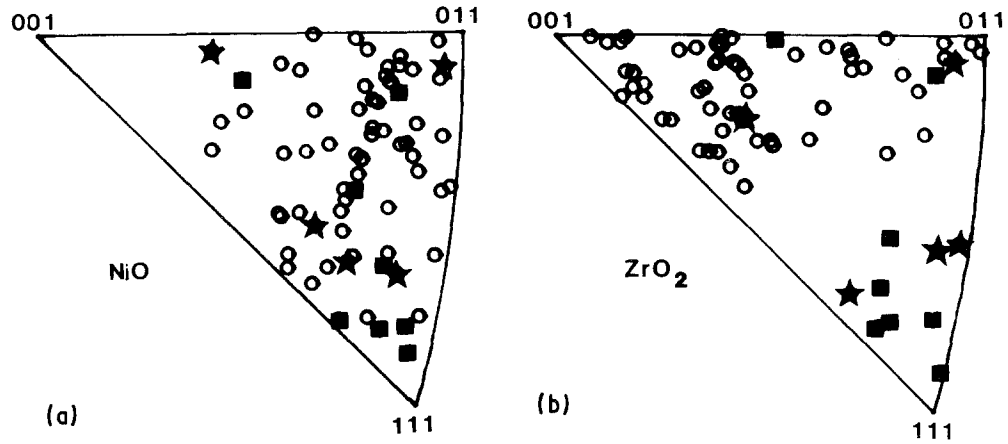

Figure 9 Distribution of the growth directions indexed relative to NiO and ZrO_2. Lamellae characterized by Relation A (○), Relation B (■), and undefined C (★).

the two phases. The interlamellar plane and growth direction were found to be $(1\,1\,1)\,NiO \parallel (1\,0\,0)\,ZrO_2$ and $[1\,\bar{1}\,0]\,NiO \parallel [0\,0\,1]\,ZrO_2$, respectively.

TEM has confirmed the existence of a large population of lamellae complying with the orientation Relation A and has given many elements for a quantitative evaluation of the homogeneity of this population which includes four out of five domains. The existence of a well-defined interlamellar plane $(1\,1\,1)\,NiO \parallel (1\,0\,0)\,ZrO_2$ was also confirmed, but no obvious preferential growth direction was observed, which indicates a behaviour similar to that reported by Echigoya *et al.* for the $MgO–ZrO_2$ eutectic [14].

TEM has allowed to evidence a second preferential orientation relation, B, characterized by $(h\,k\,l)\,[u\,v\,w]\,NiO \parallel (h\,k\,l)\,[u\,v\,w]\,ZrO_2$ which describes about 11% of the domains. Despite the slight trend in favour of $(0\,1\,1)$ as interlamellar plane and $[1\,1\,1]$ as growth direction observed, the scatter of the indices for both interface plane and growth direction is considerable and explains, together with the low proportion of such domains, why population B was undetected by X-ray diffraction.

Acknowledgement

The authors thank Dr F. d'Yvoire for helpful comments.

References

1. L. M. HOGAN, R. W. KRAFT and F. D. LEMKEY, "Eutectic grains in Advances in Materials Research", Vol. 5, edited by H. Herman (Wiley Interscience, London, 1971) p. 83.
2. V. S. STUBICAN and R. C. BRADT, "Annual Review of Materials Science", Vol. 11, edited by R. A. Huggins, R. H. Bube and D. A. Vermilyea (Annual Reviews Inc., Palo Alto, 1981) p. 267.
3. A. REVCOLEVSCHI, "Materials Science Research", Vol. 20, edited by R. E. Tressler, G. L. Messing, C. G. Pantano and R. E. Newham (Plenum, New York, 1986) p. 115.
4. *Idem, Rev. Int. Hautes Temp. Refract.* **7** (1970) 78.
5. G. DHALENNE and A. REVCOLEVSCHI, *J. Crystal Growth* **69** (1984) 616.
6. J. D. HUNT and K. A. JACKSON, *Trans. AIME* **236** (1966) 843.
7. D. D. DOUBLE, *Mater. Sci. Engng* **11** (1973) 325.
8. B. J. PLETKA, "Materials Science Research", Vol. 20, edited by R. E. Tressler, G. L. Messing, C. G. Pantano and R. E. Newnham (Plenum, New York, 1986) p. 131.
9. J. D. HUNT and K. A. JACKSON, *Trans. AIME* **236** (1966) 864.
10. A. REVCOLEVSCHI, G. DHALENNE and F. d'YVOIRE, *J. Physique C4* **46** (1985) 441.
11. M. FRAGNEAU, A. REVCOLEVSCHI and D. MICHEL, *J. Amer. Ceram. Soc.* **65** (1982) C-102.
12. J. ECHIGOYA and H. SUTO, "Grain Boundary Structure and Related Phenomena", in Proceedings of JIMIS-4, Supplement to *Trans. Jpn Inst. Met.* (1986) 213.
13. A. REVCOLEVSCHI, B. DUBOIS, G. DHALENNE and F. d'YVOIRE, *ibid.* (1986) 1045.
14. J. ECHIGOYA, H. SUTO and S. HAYASHI, *Trans. Jpn Inst. Met.* **26** (1985) 895.
15. F. F. LANGE, *Acta Metall.* **15** (1966) 311.
16. T. KARAKOSTAS, G. NOUET, G. L. BLERIS, S. HAGEGE and P. DELAVIGNETTE, *Phys. Status Solidi A* **50** (1978) 703.
17. G. FONTAINE and A. ROCHER, *J. Microsc. Electron.* **4** (1979) 19.
18. F. BARBIER, A. MARROUCHE and M. DECHAMPS, "Material Science Research", Vol. 21, edited by Pask and Evans (Plenum, New York, 1987) p. 231.
19. G. L. BLERIS, J. G. ANTONOPOULOS, T. KARAKOSTAS and P. DELAVIGNETTE, *Phys. Status Solidi* **67** (1981) 249.
20. M. DECHAMPS, F. BARBIER and A. MARROUCHE, *Acta Metall.* **35** (1987) 101.
21. A. MARROUCHE, Thesis, Université Paris-Sud, Orsay, France (July 1985).

Received 3 August
and accepted 22 October 1987